

# Damage investigation on tungsten and diamond diffractive optics at a hard x-ray free-electron laser

Fredrik Uhlén,<sup>1,\*</sup> Daniel Nilsson,<sup>1</sup> Anders Holmberg,<sup>1</sup> Hans M. Hertz,<sup>1</sup> Christian G. Schroer,<sup>2</sup> Frank Seiboth,<sup>2</sup> Jens Patommel,<sup>2</sup> Vivienne Meier,<sup>2</sup> Robert Hoppe,<sup>2</sup> Andreas Schropp,<sup>3</sup> Hae Ja Lee,<sup>3</sup> Bob Nagler,<sup>3</sup> Eric Galtier,<sup>3</sup> Jacek Krzywinski,<sup>3</sup> Harald Sinn,<sup>4</sup> and Ulrich Vogt<sup>1</sup>

<sup>1</sup> Biomedical & X-Ray Physics, Department of Applied Physics, Royal Institute of Technology, KTH-AlbaNova, SE-106 91, Stockholm, Sweden

<sup>2</sup> Institute of Structural Physics, Technische Universität Dresden, 01062 Dresden, Germany

<sup>3</sup> SLAC National Accelerator Laboratory, 2575 Sand Hill Road, Menlo Park, CA 94025, USA

<sup>4</sup> European XFEL GmbH, Notkestraße 85, 22607 Hamburg, Germany

\*fredrik.uhlen@biox.kth.se

**Abstract:** Focusing hard x-ray free-electron laser radiation with extremely high fluence sets stringent demands on the x-ray optics. Any material placed in an intense x-ray beam is at risk of being damaged. Therefore, it is crucial to find the damage thresholds for focusing optics. In this paper we report experimental results of exposing tungsten and diamond diffractive optics to a prefocused 8.2 keV free-electron laser beam in order to find damage threshold fluence levels. Tungsten nanostructures were damaged at fluence levels above 500 mJ/cm<sup>2</sup>. The damage was of mechanical character, caused by thermal stress variations. Diamond nanostructures were affected at a fluence of 59 000 mJ/cm<sup>2</sup>. For fluence levels above this, a significant graphitization process was initiated. Scanning Electron Microscopy (SEM) and  $\mu$ -Raman analysis were used to analyze exposed nanostructures.

©2013 Optical Society of America

**OCIS codes:** (340.0340) X-ray optics; (160.4670) Optical materials; (140.2600) Free-electron lasers (FELs).

---

## References and links

1. K. J. Gaffney and H. N. Chapman, "Imaging atomic structure and dynamics with ultrafast x-ray scattering," *Science* **316**(5830), 1444–1448 (2007).
2. G. Grübel, "X-ray photon correlation spectroscopy at the European x-ray free-electron laser (XFEL) facility," *C. R. Phys.* **9**(5-6), 668–680 (2008).
3. H. N. Chapman, P. Fromme, A. Barty, T. A. White, R. A. Kirian, A. Aquila, M. S. Hunter, J. Schulz, D. P. DePonte, U. Weierstall, R. B. Doak, F. R. Maia, A. V. Martin, I. Schlichting, L. Lomb, N. Coppola, R. L. Shoeman, S. W. Epp, R. Hartmann, D. Rolles, A. Rudenko, L. Foucar, N. Kimmel, G. Weidenspointner, P. Holl, M. Liang, M. Barthelmess, C. Caleman, S. Boutet, M. J. Bogan, J. Krzywinski, C. Bostedt, S. Bajt, L. Gumprecht, B. Rudek, B. Erk, C. Schmidt, A. Hömke, C. Reich, D. Pietschner, L. Strüder, G. Hauser, H. Gorke, J. Ullrich, S. Herrmann, G. Schaller, F. Schopper, H. Soltau, K. U. Kühnel, M. Messerschmidt, J. D. Bozek, S. P. Hau-Riege, M. Frank, C. Y. Hampton, R. G. Sierra, D. Starodub, G. J. Williams, J. Hajdu, N. Timneanu, M. M. Seibert, J. Andreasson, A. Rocker, O. Jönsson, M. Svenda, S. Stern, K. Nass, R. Andritschke, C. D. Schröter, F. Krasniqi, M. Bott, K. E. Schmidt, X. Wang, I. Grotjohann, J. M. Holton, T. R. Barends, R. Neutze, S. Marchesini, R. Fromme, S. Schorb, D. Rupp, M. Adolph, T. Gorkhover, I. Andersson, H. Hirsemann, G. Potdevin, H. Graafsma, B. Nilsson, and J. C. Spence, "Femtosecond X-ray protein nanocrystallography," *Nature* **470**(7332), 73–77 (2011).
4. H. C. Kang, H. Yan, R. P. Winarski, M. V. Holt, J. Maser, C. Liu, R. Conley, S. Vogt, A. T. Macrander, and G. B. Stephenson, "Focusing of hard x-rays to 16 nanometers with a multilayer Laue lens," *Appl. Phys. Lett.* **92**(22), 221114 (2008).
5. C. G. Schroer, O. Kurapova, J. Patommel, P. Boye, J. Feldkamp, B. Lengeler, M. Burghammer, C. Riekel, L. Vinze, A. van der Hart, and M. Küchler, "Hard x-ray nanoprobe based on refractive x-ray lenses," *Appl. Phys. Lett.* **87**(12), 124103 (2005).
6. H. Mimura, S. Handa, T. Kimura, H. Yumoto, D. Yamakawa, H. Yokoyama, S. Matsuyama, K. Inagaki, K. Yamamura, Y. Sano, K. Tamasaku, Y. Nishino, M. Yabashi, T. Ishikawa, and K. Yamauchi, "Breaking the 10nm barrier in hard-x-ray focusing," *Nat. Phys.* **6**(2), 122–125 (2010).

7. M. Young, "Zone plates and their aberrations," *J. Opt. Soc. Am.* **62**(8), 972 (1972).
8. P. Charalambous, I. McNulty, C. Eyberger, and B. Lai, "Developments in the fabrication of zone plates and other nanostructures," *AIP Conf. Proc.* **1365**, 65–68 (2011).
9. Y. Feng, M. Feser, A. Lyon, S. Rishton, X. Zeng, S. Chen, S. Sassolini, and W. Yun, "Nanofabrication of high aspect ratio 24 nm x-ray zone plates for x-ray imaging applications," *J. Vac. Sci. Technol. B* **25**(6), 2004 (2007).
10. J. Vila-Comamala, S. Gorelick, E. Färm, C. M. Kewish, A. Diaz, R. Barrett, V. A. Guzenko, M. Ritala, and C. David, "Ultra-high resolution zone-doubled diffractive X-ray optics for the multi-keV regime," *Opt. Express* **19**(1), 175–184 (2011).
11. D. Nilsson, F. Uhlén, J. Reinspach, H. M. Hertz, A. Holmberg, H. Sinn, and U. Vogt, "Thermal stability of tungsten zone plates for focusing hard x-ray free-electron laser radiation," *New J. Phys.* **14**(4), 043010 (2012).
12. C. David, S. Gorelick, S. Rutishauser, J. Krzywinski, J. Vila-Comamala, V. A. Guzenko, O. Bunk, E. Färm, M. Ritala, M. Cammarata, D. M. Fritz, R. Barrett, L. Samoylova, J. Grünert, and H. Sinn, "Nanofocusing of hard X-ray free electron laser pulses using diamond based Fresnel zone plates," *Sci Rep* **1**, 57 (2011), doi:10.1038/srep00057.
13. D. Nilsson, A. Holmberg, H. Sinn, and U. Vogt, "Computer simulation of heat transfer in zone plate optics exposed to x-ray FEL radiation," *Proc. SPIE* **8077**, 80770B–180770B-8 (2011).
14. F. Uhlén, S. Lindqvist, D. Nilsson, J. Reinspach, U. Vogt, H. M. Hertz, A. Holmberg, and R. Barrett, "New diamond nanofabrication process for hard x-ray zone plates," *J. Vac. Sci. Technol. B* **29**(6), 06FG03 (2011).
15. P. V. Huong, "Structural studies of diamond films and ultrahard materials by Raman and micro-Raman spectroscopies," *Diamond Related Materials* **1**(1), 33–41 (1991).
16. A. C. Ferrari and J. Robertson, "Resonant Raman spectroscopy of disordered, amorphous, and diamondlike carbon," *Phys. Rev. B* **64**(7), 075414 (2001).
17. J. Chalupský, J. Krzywinski, L. Juha, V. Hájková, J. Cihelka, T. Burian, L. Vysín, J. Gaudin, A. Gleeson, M. Jurek, A. R. Khorsand, D. Klinger, H. Wabnitz, R. Sobierajski, M. Störmer, K. Tiedtke, and S. Toleikis, "Spot size characterization of focused non-Gaussian X-ray laser beams," *Opt. Express* **18**(26), 27836–27845 (2010).
18. M. A. Pimenta, G. Dresselhaus, M. S. Dresselhaus, L. G. Cançado, A. Jorio, and R. Saito, "Studying disorder in graphite-based systems by Raman spectroscopy," *Phys. Chem. Chem. Phys.* **9**(11), 1276–1291 (2007).
19. N. Medvedev, H. O. Jeschke, and B. Ziaja, "Nonthermal phase transitions in semiconductors induced by a femtosecond extreme ultraviolet laser pulse," *New J. Phys.* **15**(1), 015016 (2013).

## 1. Introduction

New high-brightness hard x-ray free-electron laser (XFEL) facilities offer radiation with femtosecond pulse duration and exceptional coherence enabling novel and exciting experiments in a variety of scientific fields [1–3]. Nevertheless, although the brightness of these new sources is far superior than any other one that is currently available, it is in many experiments important to additionally focus the XFEL beam down to spot diameters in the nanometer regime; especially coherent x-ray imaging of single particles (high resolution), x-ray absorption spectroscopy (fluence), or nonlinear optics in the hard x-ray regime (peak intensity). Today, there are different types of x-ray optics available which are based on different physical mechanisms like, e.g., diffraction, refraction, or reflection of x-rays [4–6]. Promising diffractive optics are Fresnel zone plates (FZPs), providing excellent resolution and a clean wavefront with negligible aberrations [7]. However, the extremely high fluence imposed on zone plates from an XFEL beam can be problematic. Any structural changes in the zone plate material, caused directly by ionizing radiation or heating through absorption, could result in a decreased performance or even failure of the device.

High-Z materials, e.g., tungsten [8], gold [9], and iridium [10], are commonly used for hard x-ray zone plates as they provide high diffraction efficiencies and fairly simple fabrication methods exist. However, these metals efficiently absorb x-ray radiation which leads to a strong heating of the material. The temperature increase of the material exposed to an unfocused XFEL beam may be as high as many hundreds of Kelvins [11]. For this reason XFEL applications require metal zone plates placed on a substrate with good thermal conductivity, e.g., diamond. As reported in a previous study [11], tungsten zone plates which are bonded to a diamond substrate survive in the unfocused XFEL beam without damage.

However, an increased x-ray fluence, e.g., by prefocusing the beam, will result in higher temperatures in the zone plate material and larger temperature fluctuations between subsequent XFEL pulses. This could result in higher stress and strain variations in the material, possibly inducing mechanical fatigue. An interesting alternative is to produce combined metal-diamond zone plates, where both the high-Z metal and the diamond have been structured and are in close contact. These zone plates benefit from both the high diffraction efficiency of the high-Z metal and from the excellent heat dissipation of diamond.

David *et. al.* [12] have demonstrated that iridium-filled diamond zone plates remain undamaged when exposed to an unfocused XFEL beam.

However, at future XFEL facilities with very high fluence and high repetition rates, like the European XFEL, high-Z materials will most likely not be able to survive the XFEL beam for a long time. Instead, low-Z materials, e.g., diamond, are considered suitable [13]. Diamond with its low absorption and excellent thermal conductivity dramatically increases the damage threshold fluence.

In this paper we present experimental results from the Linac Coherent Light Source (LCLS) where tungsten and diamond diffractive optics were exposed to an 8.2 keV, prefocused XFEL beam, demonstrating at what fluence levels each of the optics degrades. These results will provide guidance for future design of XFEL diffractive optics instrumentation.

## 2. Fabrication of tungsten and diamond diffractive optics

Tungsten and diamond nanostructures were fabricated from identical multi-layer material stacks. A resist put on top of the stack was patterned using electron-beam lithography. The exposed pattern was transferred to the tungsten and diamond layers via reactive ion etching (RIE) [14].

### 2.1. Tungsten nanostructures

Tungsten nanostructures are prepared in a trilayer process. First, a tungsten layer of 1  $\mu\text{m}$  thickness is sputter-deposited onto a 100  $\mu\text{m}$  thick CVD diamond substrate (Diamond Materials GmbH). A thin chromium layer of 30 nm thickness is electron-beam evaporated onto the tungsten, and a 100 nm thick positive e-beam resist (Zep 7000, Zeon Chemicals L.P.) is subsequently spin-coated on top of the stack. The sample is exposed to a focused electron beam, which is scanned across the surface according to a predefined pattern in a direct-write electron-beam lithography step (Raith 150 system). The e-beam pattern is transferred to the chromium layer via a  $\text{Cl}_2/\text{O}_2$ -based RIE process (Oxford Instruments, Plasmalab 100 system), producing a chromium hardmask. A  $\text{SF}_6/\text{O}_2$ -based RIE step finally etches the tungsten layer, producing high aspect-ratio structures. For the damage experiment at LCLS, a matrix of tungsten zone plates with 75  $\mu\text{m}$  diameter, 50 nm outermost zone width and 300 nm - 1  $\mu\text{m}$  etch depth (line-width dependent) was fabricated. Figure 1(a) shows scanning-electron microscopy (SEM) images of fabricated tungsten nanostructures.

### 2.2. Diamond nanostructures

Diamond nanostructures are made in a similar process as tungsten, but with an additional  $\text{O}_2$ -based RIE step (Oxford Instruments, Plasmalab 80 + system). Tungsten is, in this case, used as hardmask for the diamond etch step. The diamond structures manufactured were linear gratings with a period of 200 nm and 1.4  $\mu\text{m}$  thickness. Also, a 200 nm thick tungsten layer remained on the top after the diamond etch step. Figure 1(b) displays SEM images of fabricated diamond nanostructures.

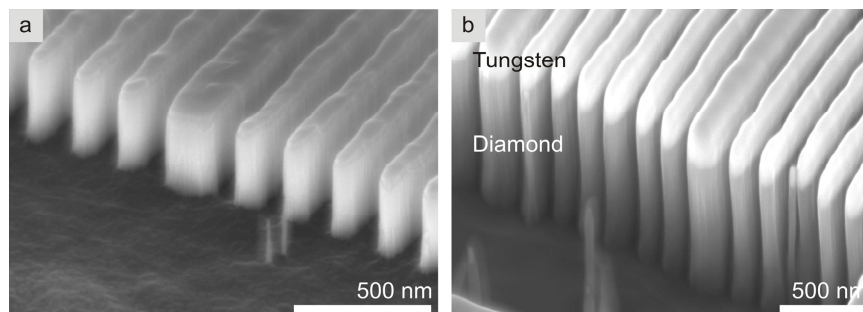


Fig. 1. (a) Tungsten nanostructures, (b) Diamond nanostructures with a thin remaining tungsten layer on the top.

### 3. Tungsten damage investigations

#### 3.1. Methods

The experiment was conducted at the Matter in Extreme Conditions (MEC) instrument at the LCLS facility. The x-ray beam had a photon energy of 8.2 keV, a pulse rate of 120 Hz, and an average energy of 1.24 mJ with a pulse duration of about 50 fs. The beamline transmission was 65%. The fluence of the unattenuated and unfocused beam in the end-station hutch was approximately 100 mJ/cm<sup>2</sup>. Exposures of samples were done in vacuum.

Figure 2 depicts the general experimental arrangement. To increase the fluence on the damage samples, a set of beryllium prefocusing lenses was used. Table 1 shows the parameters of the prefocusing lens set (Be lens stack 1) used for the tungsten zone plate sample.

**Table 1. Parameters of prefocusing beryllium lenses.**

	Pulse energy (mJ)	Number of lenses x radius of curvature (μm)	Irradiated area on sample (μm)	Total transmission	Max. fluence at sample position (mJ/cm <sup>2</sup> )
Be lens stack 1 (W)	1.24	3x100	60 x 90	0.088	2 000
Be lens stack 2 (Di)	1.24	6x300 + 1x200	Ø = 20	0.17	220 000

A pair of slits placed in front of the lenses defined a square aperture of 400 μm x 400 μm. The tungsten samples were placed downstream of the lenses so that a 90 μm x 90 μm area was illuminated. Due to the nonuniform intensity profile of the original beam, only an effective area of 60 μm x 90 μm of uniform illumination was considered for the fluence calculations. The fluence in the tungsten sample exposure is simply obtained by multiplying the incoming pulse energy with the total transmission of lenses divided by the irradiated area (fluence for diamond is obtained in another way, cf. section 4). An estimated fluence of 2000 mJ/cm<sup>2</sup> of the incident beam reached the sample without any attenuation filters. A scintillator-based high-resolution x-ray detector placed approximately 1 m behind the zone plate samples recorded the + 1st and -1st diffraction order. In this way it was possible to continuously monitor the diffracted intensity. A reduction in diffracted intensity would indicate a damage of optics. Moreover, a beam stop (Cu-wire) placed right before the microscope stopped the direct XFEL beam.

Four different tungsten zone plates were exposed to 10<sup>5</sup> pulses at 27%, 45%, 77%, and 100% of the total beam intensity, respectively, corresponding to fluence levels of 500, 900, 1600, and 2000 mJ/cm<sup>2</sup>. Attenuation of the XFEL beam was accomplished with silicon attenuators of varying thicknesses. Besides looking at the diffraction efficiency during the experiment, exposed samples were analyzed afterwards for damage with SEM.

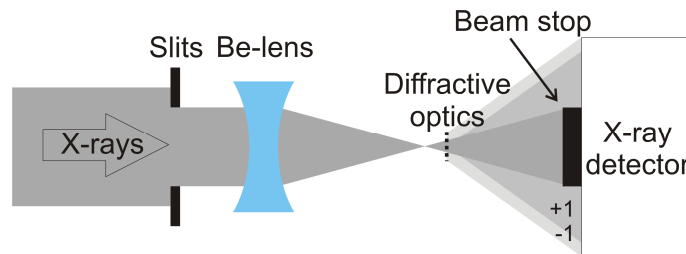


Fig. 2. Experimental arrangement for the damage experiment at LCLS. Damage samples were placed in the prefocused XFEL beam and the diffracted intensity (+ 1 and -1 orders) could be monitored during exposure.

#### 3.2. Results and discussion

In Fig. 3 SEM images demonstrate the results of the tungsten zone plate samples exposures. At 500 mJ/cm<sup>2</sup> fluence, see Fig. 3(a), no visible damage is observed. At 900 mJ/cm<sup>2</sup> fluence,

see Figs. 3(b) and 3(e), small areas in the outer regions of the zone plate indicate some initial damage. Since it is reasonable to believe that small structures are more susceptible to damage such behavior was expected. At increased fluence, 1600 and 2000  $\text{mJ}/\text{cm}^2$ , damage is obvious, see Figs. 3(c) and 3(d). Large areas of the zone plates have been destroyed and the tungsten material has even vanished. Figures 3(e) and 3(f) display close-up SEM images of damaged areas that still remain on the substrate. Visual inspection reveals that the failure is of mechanical origin rather than melting. This can be explained by stress and strain imposed on the structures due to the rapid thermal fluctuations caused by the intense beam.

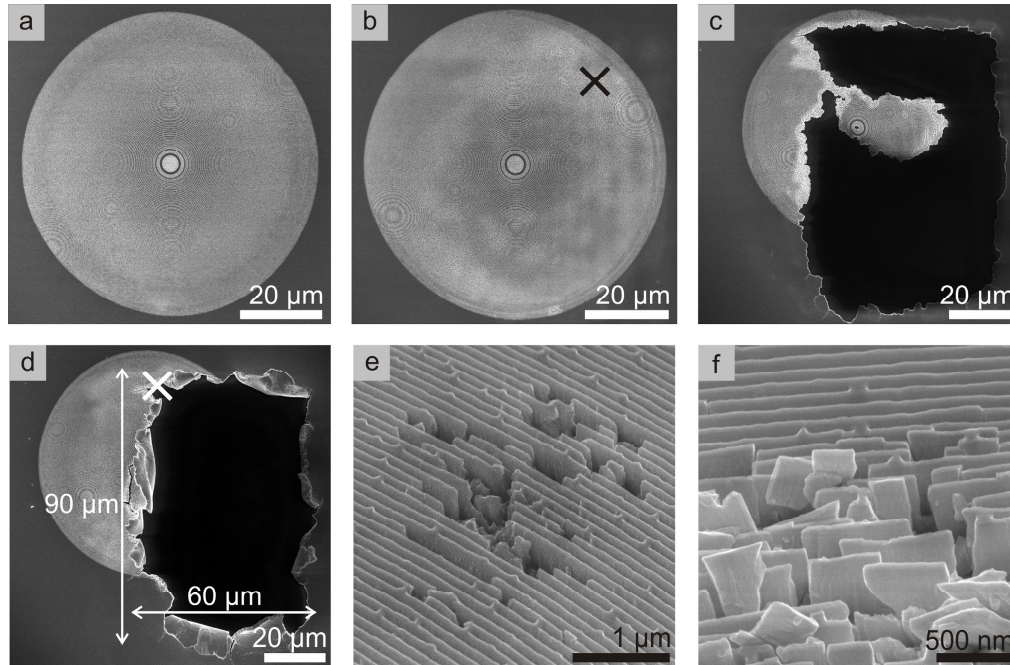


Fig. 3. SEM images of tungsten zone plates exposed to  $10^5$  single pulses at (a)  $500 \text{ mJ}/\text{cm}^2$  - no damage observed, (b)  $900 \text{ mJ}/\text{cm}^2$  fluence - some damaged areas observed in the lower and outermost part of the zone plate, cross indicates position in (e), (c)  $1600 \text{ mJ}/\text{cm}^2$  fluence - structures totally destroyed, (d)  $2000 \text{ mJ}/\text{cm}^2$  fluence - structures totally destroyed, cross indicates position in (f), arrows indicate size of the irradiated area, (e) Zoomed-in on damage in (b),  $52^\circ$  tilt angle, (f) Zoomed-in on damage in (d),  $52^\circ$  tilt angle.

The recordings from the x-ray detector revealed additional information. At  $500 \text{ mJ}/\text{cm}^2$  fluence, the diffracted intensity was unchanged throughout the whole exposure. At  $900 \text{ mJ}/\text{cm}^2$  fluence, it was difficult to see any changes in intensity, most likely because only very small areas were affected by the beam. At  $1600 \text{ mJ}/\text{cm}^2$  fluence, the diffracted intensity shown in Fig. 4 was constant for a couple of thousand pulses. Then the signal from outer parts of the zone plate starts to diminish and eventually gets weaker also for the central part. This indicates that the damage initiates in the periphery of the zone plate where small structures are present.

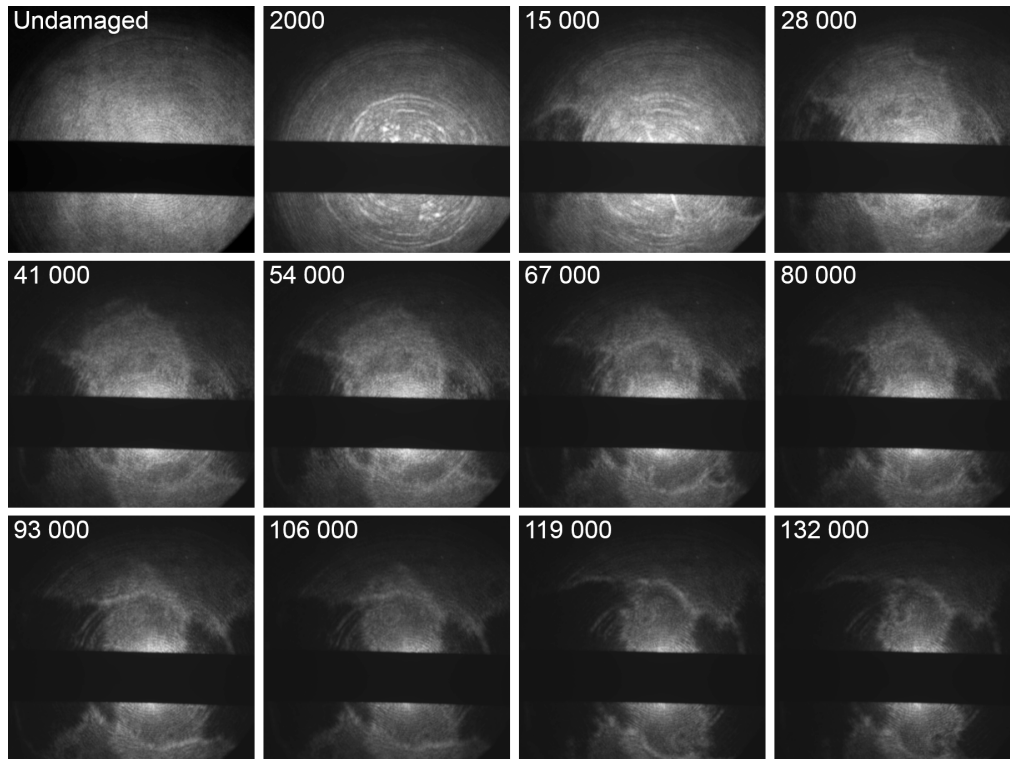


Fig. 4. Upper-left image shows diffracted intensity after 131 000 pulses at a fluence level of 500 mJ/cm<sup>2</sup> to show appearance of diffracted light from an undamaged zone plate. Other images demonstrate diffracted intensity recorded after different number of pulses at a fluence level of 1600 mJ/cm<sup>2</sup>.

**Table 2. Exposure parameters for tungsten zone plate samples.**

Fluence levels (mJ/cm <sup>2</sup> )	Average dose absorbed per atom (eV/atom)	Temperature (K)	Melting temperature (K)
500	0.15	940	3695
900	0.27	1340	
1600	0.47	2000	
2000	0.59	2430	

Our experimental findings indicate that damage initiates at a fluence level of 900 mJ/cm<sup>2</sup>. Using data on tungsten transmission and density, this fluence can be translated to an average dose absorbed per atom of 0.27 eV/atom, which is well below the melting dose of 1.5 eV/atom. The absorbed dose corresponds to a calculated temperature increase of 1300 K, which is obtained via the heat capacity of tungsten. Fluences of 1600 and 2000 mJ/cm<sup>2</sup> were also not high enough in order to initiate melting of tungsten, see Table 2. This confirms the findings from the SEM images where the damage appears not to be caused by melting, but rather by mechanical stress and strain during many heating and cooling cycles.

#### 4. Diamond damage investigations

##### 4.1 Methods

Figure 2 shows the experimental arrangement for the exposure of the diamond sample. The slit size was 600 μm x 600 μm and prefocusing was achieved with Be lens stack 2 (cf. Table 1), resulting in an illuminated area of approximately 20 μm x 20 μm at sample position. To obtain a reconstruction of the illumination profile and find fluence levels, an imprint series with single pulses at varying fluence levels was exposed on a flat surface on the diamond

sample with a 200 nm thick tungsten layer. Stated fluences are estimations of the maximum fluence at the center of the illuminated area, where most damage was observed. Diamond gratings were exposed to  $10^5$  pulses at fluence levels of 59 000, 99 000, and 220 000  $\text{mJ}/\text{cm}^2$ . The x-ray detector downstream recorded the first-order diffraction intensity of the gratings.

Imprints and exposed gratings were analyzed with SEM and  $\mu$ -Raman spectroscopy to further investigate damage.  $\mu$ -Raman spectroscopy has proven to be an excellent way of characterizing structural properties of carbon materials. Studies show that samples containing different phases of carbon, i.e., diamond, graphite, and amorphous carbon, can be clearly distinguished from one another [15, 16]. Spectroscopic studies were performed with an Alpha300 R from WITec (WITec GmbH), equipped with an optical microscope and a focused 532 nm laser beam (300 nm spot).

To further investigate the effect of thermal heating on diamond, diamond control samples (without tungsten) were annealed at 1300, 1470, 1800, and 1940 K. Annealing was performed in inert (Ar) atmosphere. For temperatures up to 1470 K substrates were annealed for 20 minutes in an Ulvac-Riko Mila 5000 furnace, and for higher temperatures substrates were annealed for approximately 30 minutes in an Activator 150 furnace. Annealed samples were investigated with  $\mu$ -Raman spectroscopy.

#### 4.2 Results of imprints

Figure 5(a), 5(b), and 5(c) depict single-pulse imprints at three different attenuation levels. From the patterns it can be seen that the intensity profile of the prefocused beam in the sample plane is clearly inhomogeneous. This can be explained by imperfections in the shape of the prefocusing lenses introduced by manufacturing errors and variations in the XFEL illumination. The beam intensity distribution at sample position was determined by an imprint technique where a series of single-pulse imprints in tungsten was recorded. The intensity in consecutive imprints was varied by changing the beamline transmission by a set of solid silicon attenuators. The outline of the area in which the tungsten has melted in each imprint can be used to create a contour map of the intensity, where each contour line has a height proportional to the inverse of the beamline transmission in that imprint. Finally this intensity map is normalized to have a total energy equal to the known pulse energy incident on the sample [17]. Figure 5(d) shows the result.

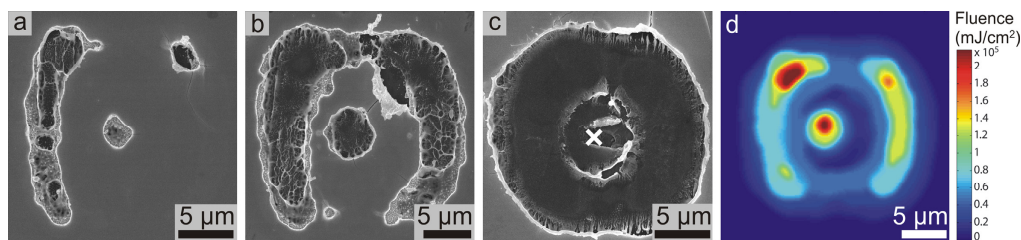


Fig. 5. Single-pulse imprints. (a) Imprint at 59 000  $\text{mJ}/\text{cm}^2$ , (b) Imprint at 99 000  $\text{mJ}/\text{cm}^2$ , (c) Imprint at 170 000  $\text{mJ}/\text{cm}^2$ , diamond is damaged in the center of the imprint. Cross indicates position for  $\mu$ -Raman spectroscopy, (d) Reconstructed beam intensity profile.

#### 4.3 Results and discussion of exposed diamond nanostructures

Figure 6 displays SEM images of exposed diamond structures at a fluence of 59 000, 99 000, and 220 000  $\text{mJ}/\text{cm}^2$ , respectively. At 59 000  $\text{mJ}/\text{cm}^2$  fluence (Fig. 6(a)), the tungsten layer has evaporated, but no crater is observed. However, the nanostructures have tilted and joined, resulting in lower spatial frequencies. This is in agreement with detected diffracted intensities corresponding to lower-frequency positions. Hence, even at this fluence level structures were affected by the beam. At 99 000 and 220 000  $\text{mJ}/\text{cm}^2$  fluence, the tungsten layer has evaporated and craters in the structures are clearly visible, as seen in Fig. 6(b) and 6(c). Figure 6(d) shows a close-up of the crater in (c). Here the grating structure has partially vanished and the remains are distorted and believed to have undergone a phase transition, see

below. However, outside the crater's center there are regions where the gratings look unaffected by the exposure (indicated by dashed lines in Figs. 6(b) and 6(c)). It was also noticed that at these fluences the diffracted intensity, measured with the x-ray detector, in the center of the exposed grating decreased during exposure, indicating structural damage.

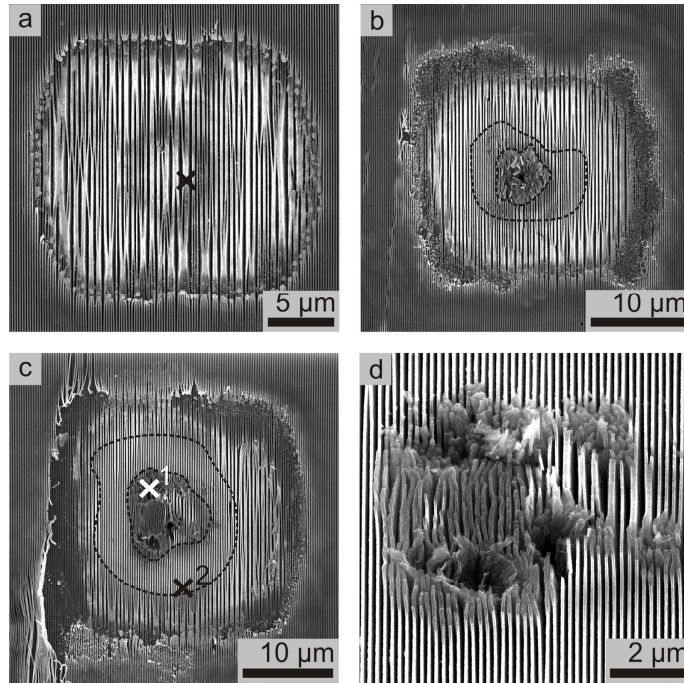


Fig. 6. Tungsten-coated diamond gratings exposed to  $10^5$  single pulses at (a) 59 000  $\text{mJ}/\text{cm}^2$  fluence - tungsten vanished, but gratings survived, (b) 99 000  $\text{mJ}/\text{cm}^2$  fluence - damage observed, (c) 220 000  $\text{mJ}/\text{cm}^2$  fluence - damage observed, (d) close-up of the damaged area in (c),  $52^\circ$  tilt angle. Crosses in figures (a) and (c) indicate position for  $\mu$ -Raman spectroscopy.

It is possible that the initial tungsten layer has an effect on the observed damage to the diamond gratings. For the lower fluences it is likely that the diamond surface was in contact with a hot tungsten layer before evaporation occurred. If the tungsten did not directly evaporate from the surface, but instead melted and solidified again a couple of times before vanishing, this process could have caused stress and strain in the gratings, resulting in the tilting of structures. At the lowest fluence level this tungsten phase cycle may have been present over the whole focus region, which would explain why most of the gratings have tilted.

The highest fluences were high enough to melt and evaporate all tungsten in a single pulse. According to the high-fluence imprints where the tungsten had melted, vanished, and the diamond beneath was exposed and damaged (Fig. 5(c)), the Raman-analysis showed that a phase transition had taken place. However, it was not to the same extent as in the crater-like damaged regions which had been exposed to  $10^5$  pulses. This indicates that some initial phase transition may have been caused by the present tungsten layer, but since this damage process continued after the tungsten layer had disappeared this on-going phase transition can only be explained by the interaction of the XFEL beam with diamond.

At higher fluences, the most intense regions caused a phase transition as described previously, but in the unaffected regions the fluence may not have been high enough to induce structural damage but sufficient to evaporate the tungsten very quickly, i.e., in a single pulse. The tungsten would then not have had any time to affect the gratings, and this would explain why this region looks unaffected. Further out the fluence was decreased and the

tungsten would have had time to go through several heat and cooling cycles and cause tilting in these regions.

#### 4.4 Diamond phase transition

Diamond phase transition was studied with Raman spectroscopy. Raman analysis of as-ordered (unprocessed) diamond is shown in Fig. 7. The strong peak at  $1342 \pm 4 \text{ cm}^{-1}$  is characteristic of the CVD diamond ( $\text{sp}^3$ -bonding). Raman analysis of processed diamond (subject to etching and other nanofabrication methods) was also performed, but no change from the original spectrum was observed. A spectrum from an imprint (cross in Fig. 5(c)) is seen in Fig. 7 where the tungsten had evaporated and the diamond surface had been damaged in a single pulse. A broad peak centered at  $1577 \text{ cm}^{-1}$  corresponding to graphite ( $\text{sp}^2$ -bonding) can be observed. Raman spectra of XFEL-exposed gratings are also displayed in Fig. 7. The diamond grating that had been exposed to the lowest fluence level (cross in Fig. 6(a)) was quite similar in spectrum to the unprocessed diamond substrate spectrum. However, a weak signal at  $1560\text{-}1630 \text{ cm}^{-1}$  is also seen, possibly indicating some initial graphitization. Diamond gratings with crater-like damage revealed a significant difference in spectrum appearance from undamaged grating areas. Whereas undamaged areas (cross 2 in Fig. 6(c)) mainly display the intense diamond peak at  $1342 \text{ cm}^{-1}$ , damaged areas (cross 1 in Fig. 6(c)) have a much weakened and broadened signal around  $1345 \text{ cm}^{-1}$  and an additional peak at  $1577 \text{ cm}^{-1}$  (graphite peak –  $\text{sp}^2$ -bonding), indicating that the diamond has undergone a graphitization process [15]. The peak at  $2700 \text{ cm}^{-1}$  is also characteristic of graphitic materials [18].

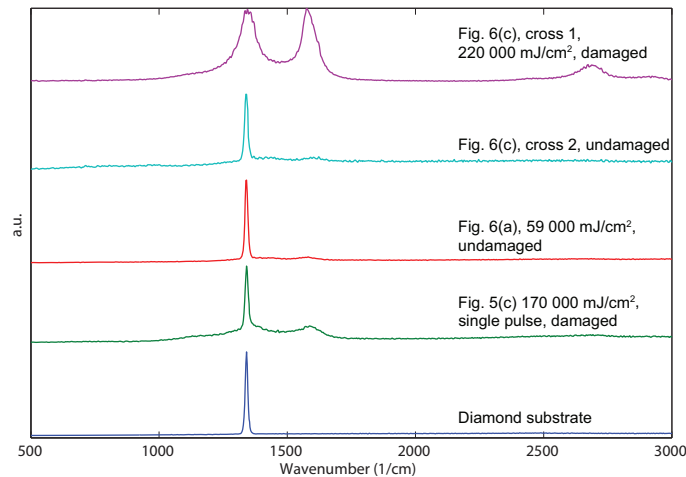


Fig. 7. Raman spectra of as-ordered (unprocessed) diamond substrate, diamond-tungsten surface exposed to a single XFEL pulse (diamond damaged), diamond-tungsten gratings exposed to XFEL beam (undamaged and damaged) at different attenuation levels. Data are normalized and shown in semi-logarithmic scale.

Results of the annealing experiment of control substrates are shown in Fig. 8. Raman analysis of diamond substrates annealed up to a temperature of 1300 K shows no significant change in spectrum from untreated substrates. At 1470 K a broad peak from 1400 to 1500  $\text{cm}^{-1}$  slowly starts to appear, which indicates a structural transformation. At 1800 K this broad peak increases, and also at 1940 K this peak is present. These results are in good agreement with the diamond manufacturers' (Diamond Materials GmbH) specifications regarding heat-induced structural transformations, which states that diamond transformations initiate at 1800 K. However, in none of these spectra is the same distinct graphite peak visible as observed for the LCLS-exposed damaged diamond gratings.

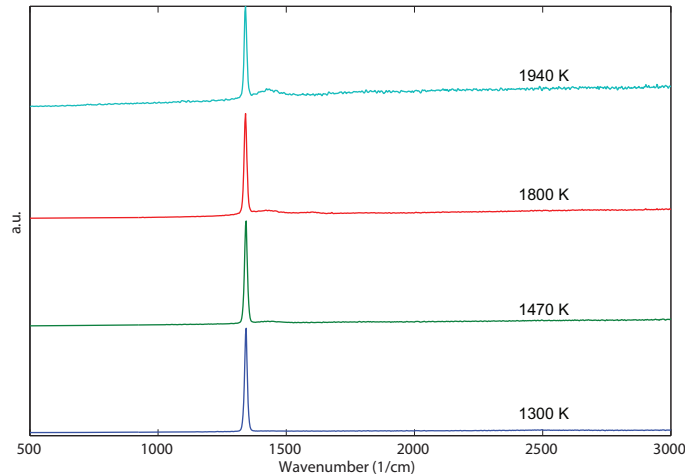


Fig. 8. Raman spectra of annealed diamond substrates at 1300, 1470, 1800, and 1940 K. Data are normalized and shown in semi-logarithmic scale.

We have also calculated the absorbed dose per atom, see Table 3. For a fluence of 59 000  $\text{mJ}/\text{cm}^2$  the average dose per atom is calculated to 0.027 eV/atom, which corresponds to a temperature increase of 280 K. At 99 000  $\text{mJ}/\text{cm}^2$  fluence the diamond structures have been damaged by the beam. The absorbed dose is calculated to 0.046 eV/atom, corresponding to a temperature increase of 400 K. The phase transition threshold fluence is found between 59 000 and 99 000  $\text{mJ}/\text{cm}^2$ . The highest fluence of 220 000  $\text{mJ}/\text{cm}^2$  also resulted in phase transition.

**Table 3. Exposure parameters for diamond.**

Fluence levels ( $\text{mJ}/\text{cm}^2$ )	Average dose absorbed per atom (eV/atom)	Temperature (K)	Graphitization temperature (K)
59 000	0.027	570	1800
99 000	0.046	700	
220 000	0.10	1010	

From these results some interesting observations can be made. When transferring damaging fluence levels into absorbed dose energies or temperature elevations, we notice that graphitization has occurred even though the induced heat in the diamond structures is well below the graphitization temperature. One should bear in mind that the tungsten layer may have had an effect on the diamond, but since this layer is quickly evaporated, the diamond graphitization is probably caused by the hard x-ray interaction with diamond itself. Therefore, we believe that the damage mechanism caused by the intense XFEL beam is different from damage caused by simple heating of diamond.

## 5. Summary

We have investigated the damage to tungsten and diamond diffractive optics at a free-electron laser facility (LCLS). Tungsten zone plates survived  $10^5$  pulses at a fluence of 500  $\text{mJ}/\text{cm}^2$ , and initial damage was observed at 900  $\text{mJ}/\text{cm}^2$  fluence. This should be compared with a fluence of 100  $\text{mJ}/\text{cm}^2$  delivered by the unfocused LCLS-beam. The damage was not caused by melting of the material but by disintegrating of the nanostructures, most likely caused by stress and strain during rapid heating and cooling cycles.

Diamond optics survived  $10^5$  pulses at a fluence of 59 000  $\text{mJ}/\text{cm}^2$ . At this fluence level, tilting of structures was observed, assumed to be caused by the tungsten layer on top. However, structures have not been subject to graphitization. At higher fluences we observed damage to the diamond material itself. The material was analyzed to contain both diamond and graphite signals, indicating graphitization at fluences higher than 59 000  $\text{mJ}/\text{cm}^2$ . However, the calculated temperature increase in the diamond at the highest fluence levels was

not sufficient to overcome the thermally induced graphitization barrier. Instead, the experiment indicates that the transformation process is better described as a nonthermal transition or a combination of temperature and radiation damage caused by a high intensity, ultrashort hard x-ray FEL beam. Medvedev *et. al.* [19] also predicts nonthermal phase transitions for diamond using ultrashort EUV laser pulses, which further supports our conclusion.

### **Acknowledgments**

This work was funded by the Swedish Research Council and the Göran Gustafsson foundation. The experiment was performed at the Linac Coherent Light Source (LCLS) at SLAC National Accelerator Laboratory. LCLS is a national user facility operated by Stanford University on behalf of the U.S. Department of Energy, Office of Basic Energy Sciences. The MEC instrument was supported by U.S. Department of Energy, Office of Fusion Energy Sciences. We would like to thank Birgit Brandner at YKI for performing  $\mu$ -Raman spectroscopy measurements. Also, thanks to Anastasia Riazanova at KTH MSE and Arman Sikiric at Acreo for annealing diamond samples.